Cleanliness of Ti-bearing Al-killed ultra-low-carbon steel during different heating processes

Jian-long Guo, Yan-ping Bao, and Min Wang

State Key Laboratory of Advanced Metallurgy, University of Science and Technology Beijing, Beijing 100083, China

Abstract: During the production of Ti-bearing Al-killed ultra-low-carbon (ULC) steel, two different heating processes were used when the converter tapping temperature or the molten steel temperature in the Ruhrstahl–Heraeus (RH) process was low: heating by Al addition during the RH decarburization process and final deoxidation at the end of the RH decarburization process (process-I), and increasing the oxygen content at the end of RH decarburization, heating and final deoxidation by one-time Al addition (process-II). Temperature increases of 10°C by different processes were studied; the results showed that the two heating processes could achieve the same heating effect. The T.[O] content in the slab and the refining process was better controlled by process-I than by process-II. Statistical analysis of inclusions showed that the numbers of inclusions in the slab obtained by process-I were substantially less than those in the slab obtained by process-II. For process-I, the Al$_2$O$_3$ inclusions produced by Al added to induce heating were substantially removed at the end of decarburization. The amounts of inclusions were substantially greater for process-II than for process-I at different refining stages because of the higher dissolved oxygen concentration in process-II. Industrial test results showed that process-I was more beneficial for improving the cleanliness of molten steel.

Keywords: low carbon steel; cleanliness; RH process; heating; inclusions

1. Introduction

Ti-bearing Al-killed ultra-low-carbon (ULC) steel is often used for home appliances and automobiles and has very high cleanliness and surface quality requirements of the slab. Large nonmetallic inclusions in steel are the main source of defects in cold-rolled steel plates [1–5]. The main process for producing Ti-bearing Al-killed ULC steel is basic oxygen furnace (BOF) → Ruhrstahl–Heraeus (RH) reactor → continuous casting (CC). If the converter tapping temperature or the molten steel temperature during the RH process is low, the temperature should be increased via the reaction of Al and oxygen in the process to ensure that the casting temperature is reached [6]; however, this process will lead to the generation of a large number of Al$_2$O$_3$ inclusions and affect the cleanliness of steel. The Al$_2$O$_3$ and Al–O–Ti inclusions generated during the production of ULC steel lead to serious nozzle clogging [7].

Numerous studies on the cleanliness of ULC steel have been reported. Zhang and Li [8] studied the influence of Ti on the cleanliness of ULC steel. Other researchers have reported that lower slag oxidizability is beneficial for improving the cleanliness of molten steel during the refining process [9–11]. Wang *et al.* [12] reported that coordinated control of carbon and oxygen was also beneficial for improving the cleanliness of ULC steel. However, the effect of chemical heating by Al addition, the timing of Al addition on the cleanliness of ULC steel, and the inclusion removal mechanism by Al addition before and after decarburization have not been reported. Through investigation, chemical heating has been found to account for 27.8% of ULC steel production in some steel plants. In the present work, to study the influence of different heating processes on the cleanliness of ULC steel and to determine the appropriate chemical heating process, we tracked, sampled, and analyzed the total oxygen content (T.[O]); the size, quantity, distribution, and composition of non-metallic inclusions; and the slag content during the whole smelting process.

Springer

2. Experimental

2.1. Production process and steel composition

The experiment was carried out in a 300-t RH reactor. The production process was as follows: Kanbara reactor (KR) → BOF → RH reactor → CC. The composition of the experimental steel is listed in Table 1.

Industrial experiments involved different heating processes. Process-I was heating by Al addition during the

RH decarburization process and final deoxidation at the end of RH decarburization. When using process-I, to reduce the influence of Al addition on the decarburization rate, the time of Al addition was controlled at 6 min after the vacuum started. Process-II was increasing the oxygen content at the end of RH decarburization followed by heating and final deoxidation by one-time Al addition. To ensure the consistency of the experimental results, the heating temperature was 10°C for both processes.

Table 1. Composition of the experimental steel wt%

C	Si	Mn	P	S	Al	Ti	N
≤0.0035	≤0.03	0.08–0.15	≤0.015	≤0.012	0.030–0.055	0.050–0.070	≤0.004

2.2. Sampling and analysis

In the two different heating processes, steel and slag samples were extracted during the RH refining process. Steel and slag samples were collected by pail samplers with

an inner diameter of 80 mm. The steel sampling position was located 200 mm below the slag surface. Fig. 1 shows an illustration of the alloy addition and sampling processes during the RH refining stage, where the time at which vacuum starts is assumed as 0 min.
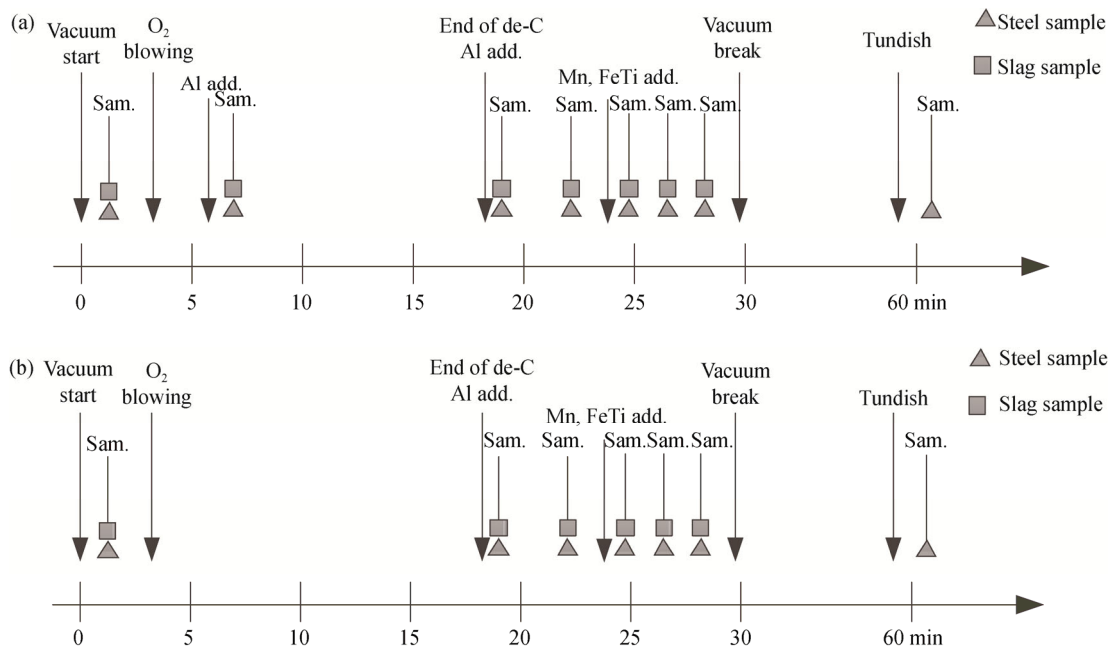

Fig. 1. Illustration of the alloy addition (add.) and sampling (sam.) processes during the RH refining process: (a) process-I; (b) process-II.

The slab was sampled at the edges, one-fourth the distance from the center to the edge in the width direction, and the center of the slab to analyze the inclusions. The T.[O] of the steel samples was analyzed using an EMGA-830 oxygen–nitrogen analyzer. The content of the slag samples was analyzed using an EDX800 X-ray fluorescence spectrometer. Inclusions on the cross-section of the steel samples were characterized using an Oxford-Inca automatic inclusion analysis system; the composition, size, and distribution of the inclusions were measured. To

ensure the accuracy and consistency of the scanning data, the scanning area was 7 mm × 7 mm. The morphology of inclusions was analyzed by scanning electron microscopy–energy-dispersive X-ray spectroscopy (SEM–EDS).

3. Results

3.1. Temperature evolution of the refining process

Fig. 2 shows the temperature evolution during the ULC

steel refining process; the tapping temperature for the heating processes was 10°C lower than that for the normal process. At 6 min after vacuum started, 88 kg of Al was added to induce heating for process-I. For the normal process and process-I, the temperature at the end of decarburization was controlled at 1590°C. When the vacuum was broken, the temperatures of the molten steel for process-I and process-II were controlled at 1586 and 1587°C, indicating that two processes achieved the same heating effect.
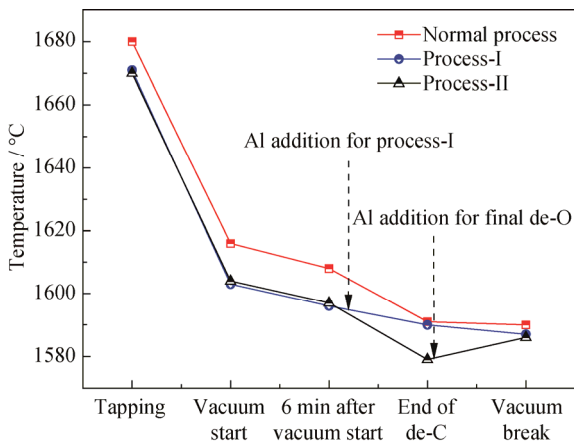

Fig. 2.   Temperature evolution of the refining process.

3.2. T.[O] evolution of the refining process

Fig. 3 shows the T.[O] evolution for all of the processes at different refining stages: the end of RH decarburization, 6 min after deoxidation by Al addition, 4 min after alloy addition, vacuum break, and in the tundish. The T.[O] content at the end of RH decarburization is an important factor affecting the cleanliness of ULC steel [13]. In process-I, the T.[O] content at the end of RH decarburization was 400 ppm, whereas the T.[O] content at the end of RH decarburization was 480 ppm in process-II, which is substantially greater than that in process-I. The T.[O] in the molten steel was effectively removed after the RH cycle treatment and sedation. The T.[O] in the tundish is another important factor affecting the cleanliness of ULC steel [2]. For process-II, the T.[O] in the tundish reached 56 ppm, which is twice as high as that for the normal process and 70% up compared with process-I. Therefore, process-I can control the T.[O] during the refining process more effectively than process-II and can improve the cleanliness of the ULC steel.

3.3. T.[O] in slab

The cleanliness of the steel can be measured on the basis of the T.[O] in the slab. The T.[O] content in the slab by different heating processes is shown in Fig. 4. To avoid the in-

fluence of sampling positions, the T.[O] values at the edge, one-fourth the distance from the center to the edge, and at the center in the slab were compared.
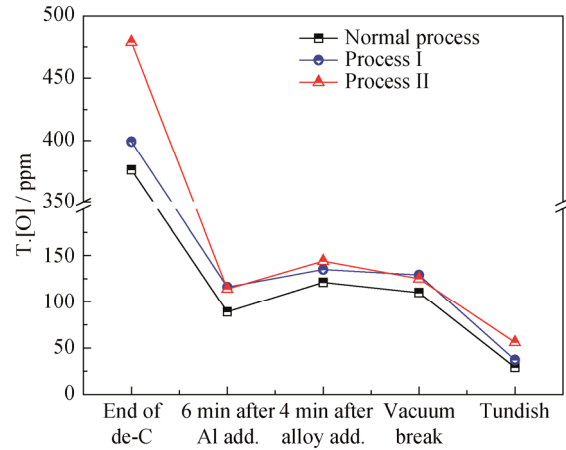

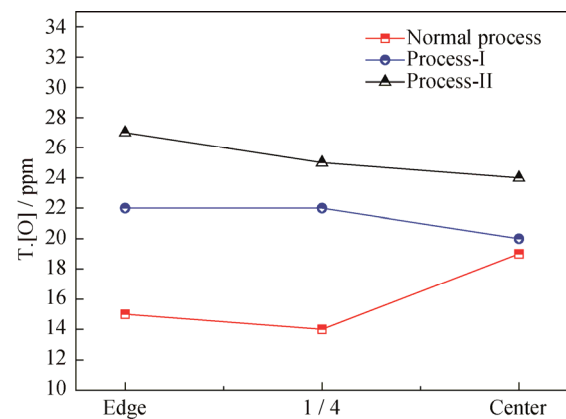**Fig. 3.   Evolution of T.[O] during the refining process.**

Fig. 4.   T.[O] in the slab by different heating processes.

As shown in Fig. 4, the T.[O] contents in the slab from the edge to the center were 15, 14, and 19 ppm in the case of the normal process; these values are lower than the T.[O] contents in the case of the heating processes. A comparison of the two different heating processes reveals that the T.[O] in the slab produced by process-I was approximately 22 ppm, whereas that in the slab produced by process-II was approximately 26 ppm. Thus, the T.[O] in the slab produced by process-I was lower than that in the slab produced by process-II.

3.4. Evolution of slag composition at different refining stages

In ULC steel, the inclusions are mainly Al_2O_3. Therefore, the slag composition should be controlled to remove Al_2O_3 inclusions from the steel. The C/A ($wCaO/wAl_2O_3$) ratio and (FeO + MnO) content are general parameters that represent

the oxidizing tendency of a slag [14–16]. To ensure that Al_2O_3 inclusions could be removed effectively, the C/A ratio in the slag was controlled between 1.2 and 2.0, and the (FeO + MnO) content was controlled below 10wt%. The slag contents at different refining stages in different processes are listed in Table 2. When vacuum started, the C/A ratio in the slag was maintained between 1.5 and 1.7 through the slag modification process and the contents of the slag of three test heats were similar. This result indicates that the oxidiza-

bility of molten steel in slag and the inclusion adsorption capacity of slag were similar in all processes. The Al_2O_3 content in the slag increased gradually with the extension of the pure degassing time, which indicates that the inclusions in molten steel were continuously floating to the top slag during the RH treatment process. In all processes, the (FeO + MnO) content generally decreased from the end of decarburization to vacuum break and the content was controlled below 8wt%.

Table 2. Slag composition at different refining stages in different processes   wt%

Process	Description	CaO	Al_2O_3	SiO_2	MgO	FeO	MnO
Normal process	Vacuum start	49.5	29.6	7.2	5.9	6.2	1.6
	End of de-C	49.8	28.6	7.9	6.1	5.8	1.9
	4 min after Al addition	49.7	29.3	7.4	6.4	4.9	2.3
	4 min after Ti addition	49.2	31.7	7.1	5.3	5.3	1.4
	Vacuum break	48.3	32.2	6.6	6.3	5.1	1.5
Process-I	Vacuum start	49.6	29.9	7.9	5.5	5.7	1.4
	End of de-C	48.7	31.6	6.4	6.1	5.3	1.9
	4 min after Al addition	48.3	33.2	6.0	5.7	5.6	1.2
	4 min after Ti addition	47.7	34.7	5.7	5.9	4.9	1.1
	Vacuum break	47.9	35.5	6.0	5.5	4.6	0.7
Process-II	Vacuum start	50.1	29.3	7.2	6.6	5.1	1.7
	End of de-C	49.7	29.5	6.6	7.3	5.0	1.9
	4 min after Al addition	48.9	30.3	7.6	5.9	5.2	1.5
	4 min after Ti addition	46.3	33.4	6.3	7.7	4.9	1.5
	Vacuum break	47.8	33.8	5.8	6.9	3.9	1.8

3.5. Inclusion size and number density distribution

The distribution of inclusions was analyzed using the Oxford-Inca inclusion analysis system; the analysis position

was one-fourth the distance from the edge to the center of the slab. The results are shown in Fig. 5, where each color represents a characteristic inclusion.
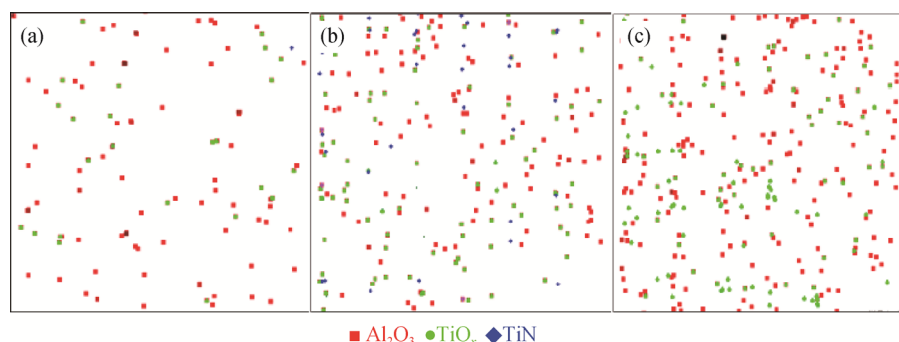

■ Al_2O_3 ● TiO_x ◆ TiN

Fig. 5.   Distribution of inclusions in slabs subjected to different heating processes: (a) normal process; (b) process-I; (c) process-II.

Fig. 5 shows that the inclusions were mainly Al_2O_3, Al_2O_3–TiO_x, TiN, and their complex inclusions; it also shows that the distribution of inclusions in the slab of

process-II was substantially greater than those of process-I and the normal process. The number distribution of Al_2O_3 and Al_2O_3–TiO_x inclusions in different sizes is shown in Figs.

6 and 7. The numbers of Al_2O_3 and Al_2O_3–TiO_x inclusions in the slab for the normal process were 118, including 92 Al_2O_3 inclusions and 26 Al_2O_3–TiO_x inclusions; by contrast, they were 156 in process-I, including 118 Al_2O_3 inclusions and 38 Al_2O_3–TiO_x inclusions, and 295 in process-II, including 237 Al_2O_3 inclusions and 58 Al_2O_3–TiO_x inclusions. A comparison of the two different heating processes and the normal process reveals that process-II resulted in 90% more inclusions than process-I and 150% more inclusions than the normal process. Al_2O_3–TiO_x inclusions can cause serious nozzle clogging [7]. Process-II resulted in 50% more Al_2O_3–TiO_x inclusions than process-I and 120% more than the normal process. Process-II resulted in greater numbers of Al_2O_3 and Al_2O_3–TiO_x inclusions larger than 4 μm than process-I and the normal process. Thus, considering the type, quantity, distribution, and size of the inclusions, the cleanliness of the slab obtained by process-I is better than that obtained by process-II.

4. Discussion

Before deoxidation, a large number of spherical or ellipsoidal (Fe,Mn)O particles are dispersed in the molten steel matrix, as shown in Fig. 8. The single-particle diameter is 1–3 μm, and a few particles gather together to form clusters.

Fig. 6.   Size distribution of Al_2O_3 inclusions in the slabs.
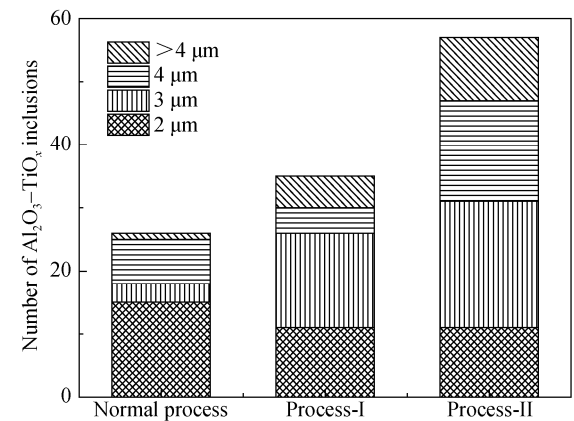
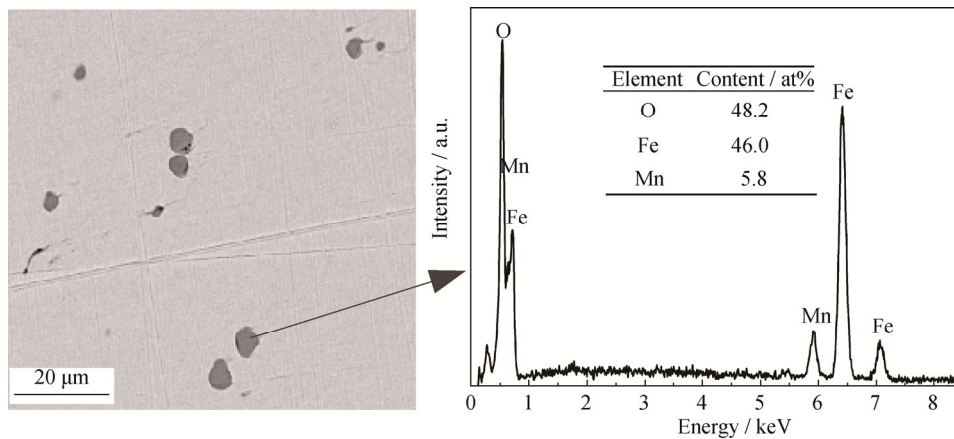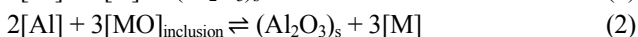**Fig. 7.   Size distribution of Al_2O_3–TiO_x inclusions in the slabs.**

Fig. 8.   SEM-EDS results of typical inclusions before deoxidation.

After the addition of Al, [Al] will react with oxygen, as shown in Eqs. (1) and (2):

$$2[Al] + 3[O] \rightleftharpoons (Al_2O_3)_s \tag{1}$$

$$2[Al] + 3[MO]_{inclusion} \rightleftharpoons (Al_2O_3)_s + 3[M] \tag{2}$$

In Eq. (2), M is Fe or Mn. In the reaction process, the main factor affecting inclusion numbers is the dissolved oxygen concentration before Al addition. The higher the dissolved oxygen concentration, the greater the Al addition and the greater the inclusion numbers [11]. Metallurgical
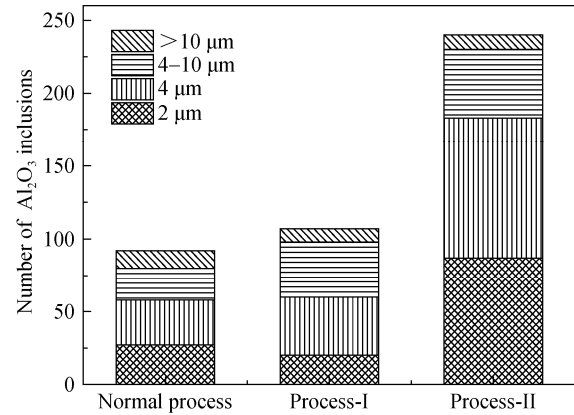
parameters associated with different test processes are listed in Table 3.

For the normal process, the dissolved oxygen concentration before final deoxidation was 389 ppm, which is higher than that in process-I. However, because the total amount of Al addition for the normal process was lower than that for process-I and process-II, the inclusion numbers for the normal process were lower than those for process-I and process-II, as mentioned in section 3.5.

Table 3.   Metallurgical parameters in different test processes

Process	Mass / t	[O] before heating / ppm	Amount of heating Al addition / kg	[O] before de-O / ppm	Amount of De-O Al addition / kg
Normal process	308	—	—	389	358
Process-I	311	475	88	359	316
Process-II	314	—	—	423	402

In process-I, Al addition was divided into two parts. Part of the Al was added during the decarburization process for heating, where the inclusions require a longer time to remove; because the dissolved oxygen in the molten steel was reduced, the inclusions produced by final deoxidation were also reduced accordingly. The distribution of the inclusions at different refining stages for process-I was analyzed. The results corresponding to 2 min after heating by Al addition at the end of the RH decarburization process are shown in Fig. 9(a). At 2 min after heating by Al addition, the main inclusions were Al_2O_3, (Fe,Mn)O, and Al_2O_3 wrapped in (Fe,Mn)O. The SEM–EDS analysis results for Al_2O_3 wrapped in (Fe,Mn)O are shown in Fig. 10. At the end of decarburization, the main inclusions were (Fe,Mn)O and the Al_2O_3 inclusions had been substantially removed in the same heat, as shown in Fig. 9(b). The numbers of inclusions at different stages are shown in Fig. 11. The Al_2O_3 and Al_2O_3 wrapped in (Fe,Mn)O inclusions at 2 min after Al addition accounted for 96.6% of the total; however, at the end of decarburization, they accounted for only 14.2% of the total for process-I. From 2 min after Al addition to the end of decarburization, the number of (Fe,Mn)O inclusions increased because of the second O_2 blowing at 4 min after Al addition to ensure decarburization. However, the removal rate of Al_2O_3 and Al_2O_3 wrapped in (Fe,Mn)O inclusions reached 72.3%. Therefore, in the case of process-I, the inclusions of Al_2O_3 and Al_2O_3 wrapped in (Fe,Mn)O were obviously removed via the molten steel cycle and the main inclusions before deoxidation were similar to those in the normal process.

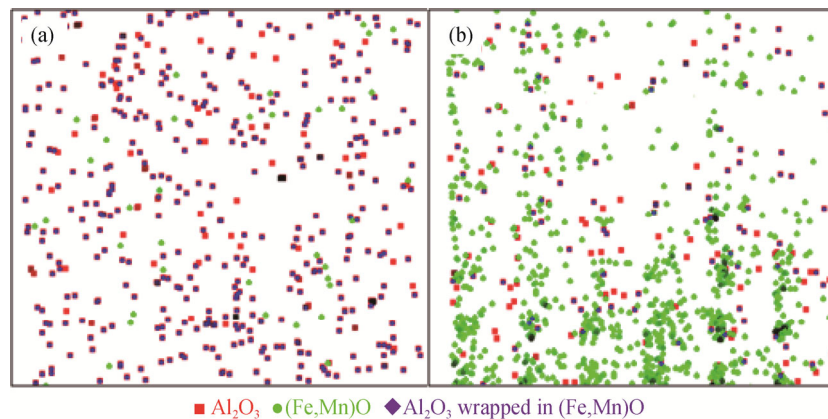■ Al_2O_3 ● (Fe,Mn)O   ◆ Al_2O_3 wrapped in (Fe,Mn)O

Fig. 9.   Distribution of inclusions at different refining stages for process-I: (a) 2 min after heating by Al addition; (b) at the end of RH decarburization.

For process-II, the dissolved oxygen before deoxidation was 423 ppm, which was significantly higher than that for process-I and the normal process. The greater dissolved oxygen content in the case of process-II indicates that more Al_2O_3 inclusions were generated. Figs. 12 and 13 show the distribution and quantity of inclusions at different refining stages for process-I and process-II: 6 min after Al addition (before Ti addition) and 6 min after Ti addition (vacuum break). The main inclusion type after Al addition is Al_2O_3, and the inclusion numbers at 6 min after Al addition for process-I and process-II are 392 and 547, respectively. The main inclusion type after Ti addition was Al_2O_3 and Al_2O_3–TiO_x complex inclusions; the Al_2O_3 and Al_2O_3–TiO_x complex inclusion numbers at 6 min after Ti addition for process-I are 217 and 58, respectively, whereas the Al_2O_3 and Al_2O_3–TiO_x complex inclusion numbers for process-II are 395 and 115, respectively. Thus, the inclusion numbers for process-I were substantially lower than those for process-II at different refining stages. Because the treatment time was the same, the oxidizability of molten steel by slag and the inclusion adsorption capacity of slag were similar for process-I and process-II, as mentioned in section 3.4; however, the inclusion numbers in molten steel for process-II were still greater. Therefore, in the case of process-I, inclusions are easier to remove, and cleanliness control is more effective.
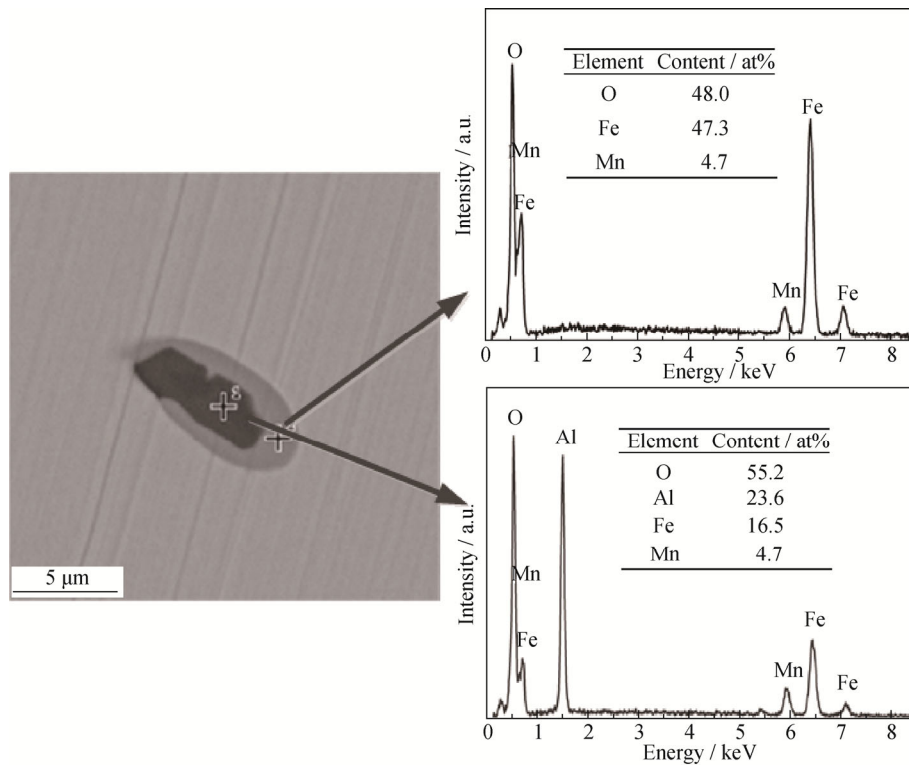
Fig. 10.   SEM–EDS analysis results for Al$_2$O$_3$ wrapped in (Fe,Mn)O after the addition of Al during the decarburization process.
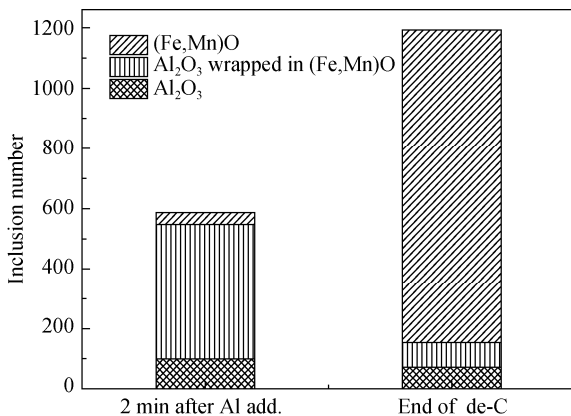

Fig. 11.   Quantitative distribution of different inclusions for process-I.

To further verify the effect of heating on the cleanness of

different processes, the T.[O] in the slab of 150 heats in industrial production were compared; the results are shown in Fig. 14. The T.[O] in the normal process was lower than that in the heating process; however, the T.[O] could be reduced from 22 to 17 ppm by using process-I compared with using process-II.

5. Conclusions

(1) For process-I and process-II, the same heating effect could be achieved.

(2) A comparison of the T.[O] and inclusion numbers of the two heating processes revealed that the T.[O] content in the slab was lower in the case of process-I. Process-II resulted in greater numbers of Al$_2$O$_3$ inclusions and Al$_2$O$_3$–TiO$_x$ inclusions than process-I and the normal process.
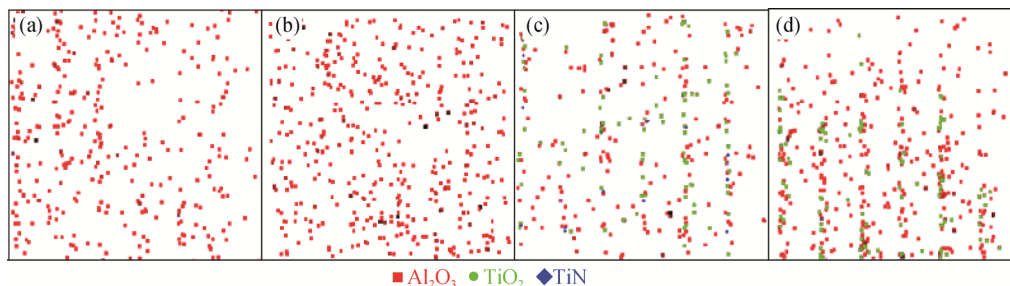

Fig. 12.   Distribution of inclusions at different refining stages: (a) 6 min after Al addition for process-I; (b) 6 min after Al addition for process-II; (c) 6 min after Ti addition for process-I; (d) 6 min after Ti addition for process-II.
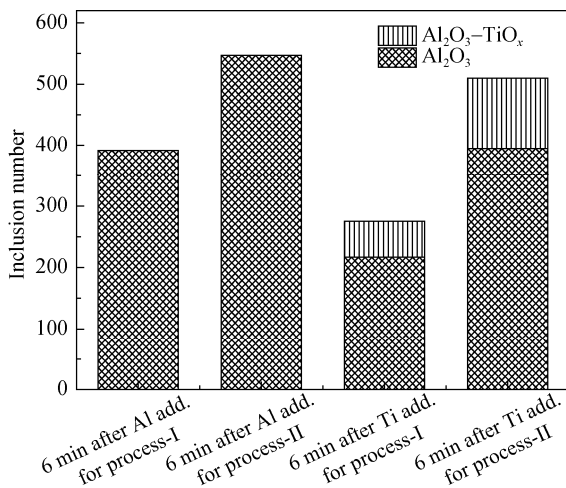
Fig. 13. Quantities of inclusions for process-I and process-II.
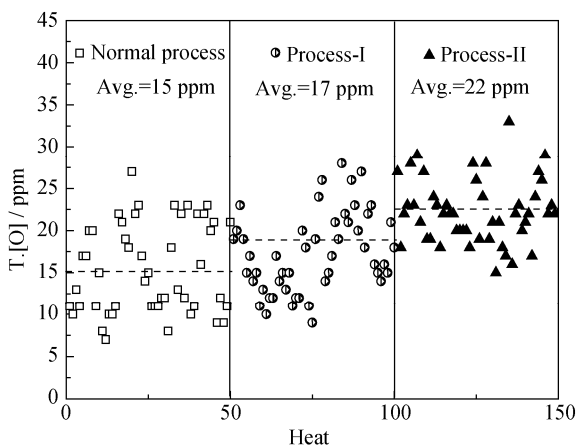

Fig. 14. Comparison of the T.[O] for the normal process, process-I, and process-II.

(3) For the normal process, because the total amounts of Al added were substantially lower than the amounts added during process-I and process-II, the normal process resulted in fewer inclusions. For process-I, inclusions were easier to remove via heating by Al addition, and the removal rate of Al_2O_3 inclusions at the end of decarburization reached 72.3%. For process-II, because the concentration of dissolved oxygen at the end of decarburization was higher than that in process-I, the inclusion numbers were substantially greater than those in process-I at different refining stages.

(4) Industrial production results showed that T.[O] could be reduced from 22 to 17 ppm by using process-I compared with using process-II and that process-I was more beneficial for improving the cleanliness of molten steel.

Acknowledgement

References

[1] H. Tsunekawa, T. Yamashita, T. Aoyama, and R. Sugihara, Mechanism of formation of streak-shaped defects on ultra-low carbon IF steel for automobile outer panels after press forming and influence of slab reheating temperature before hot rolling and Sb-addition on defects, *Tetsu-to-Hagane*, 102(2016), No. 4, p. 202.

[2] P. Palai, P.P. Sahoo, A. Dey, T.K. Roy, and V.V. Mahashabde, Constitutional segregation of Al_2O_3, in mold slag and its impact on steel cleanliness during continuous casting, *Metall. Mater. Trans. B*, 44(2013), No. 5, p. 1185.

[3] J.O. Jo, W.Y. Kim, D.S. Kim, and J.J. Pak, Thermodynamics of titanium, nitrogen, and oxygen in liquid alloy steels, *Met. Mater. Int.*, 14(2008), No. 4, p. 531.

[4] Y.M. Qin, X.H. Wang, F.X. Huang, B. Chen, and C.X. Ji, Influence of reoxidation by slag and air on inclusions in IF steel, *Metall. Res. Technol.*, 112(2015), No. 4, art. No. 405.

[5] E. Gutiérrez, S. Garcia-Hernandez, and J.D.J. Barreto, Mathematical analysis of the dynamic effects on the deposition of alumina inclusions inside the upper tundish nozzle, *ISIJ Int.*, 56(2016), No. 8, p. 1394.

[6] P.H. Li, Y.P. Bao, F. Yue, and J. Huang, BOF end-point control of ultra low carbon steel, *Iron Steel*, 46(2011), No. 10, p. 27.

[7] S. Basu, S.K. Choudhary, and N.U. Girase, Nozzle clogging behaviour of Ti-bearing Al-killed ultra low carbon steel, *ISIJ Int.*, 44(2004), No. 10, p. 1653.

[8] F. Zhang and G.Q. Li, Control of ultra low titanium in ultra low carbon Al−Si killed steel, *J. Iron Steel Res. Int.*, 20(2013), No. 4, p. 20.

[9] Y.M. Qin, X.H. Wang, L.P. Li, and F.X. Huang, Effect of oxidizing slag on cleanliness of IF steel during ladle holding process, *Steel Res. Int.*, 86(2015), No. 9, p. 1037.

[10] C.Y. Liu, F.X. Huang, and X.H. Wang, The effect of refining slag and refractory on inclusion transformation in extra low oxygen steels, *Metall. Mater. Trans. B*, 47(2016), No. 2, p. 999.

[11] E. Zinngrebe, C.V. Hoek, H. Visser, A. Westendorp, and I.H. Jung, Inclusion population evolution in Ti-alloyed Al-killed

steel during secondary steelmaking process, *ISIJ. Int.*, 52(2012), No. 1, p. 52.

[12] M. Wang, Y.P. Bao, Q. Yang, L.H. Zhao, and L. Lu, Coordinated control of carbon and oxygen for ultra-low-carbon interstitial-free steel in a smelting process, *Int. J. Miner. Metall. Mater.*, 22(2015), No. 12, p. 1252.

[13] W.C. Doo, D.Y. Kim, S.C. Kang, and K.W. Yi, The morphology of Al−Ti−O complex oxide inclusions formed in an ultra low-carbon steel melt during the RH process, *Met. Mater. Int.*, 13(2007), No. 3, p. 249.

[14] W. Yang, X.H. Wang, L.F. Zhang, Q.L. Shan, and X.F. Liu, Cleanliness of low carbon aluminum-killed steels during secondary refining processes, *Steel Res. Int.*, 84(2013), No. 5, p. 473.

[15] B.H. Yoon, K.H. Heo, J.S. Kim, and H.S. Sohn, Improvement of steel cleanliness by controlling slag composition, *Ironmaking Steelmaking*, 29(2002), No. 3, p. 214.

[16] M.K. Sun, I.H. Jung, and H.G. Lee, Morphology and chemistry of oxide inclusions after Al and Ti complex deoxidation, *Met. Mater. Int.*, 14(2008), No. 6, p. 791.